photonics

MDPI

Article

Microscale Yarn Stress Distribution Mechanism in Sheared Kevlar Plain-Woven Fabrics Revealed by Micro-Raman Spectroscopy

Fuyong Qin [1,2], Xinmin Fan [1,2,3,*], Yu Ma [4,*], Jianxin Zhang [1,2], Zaifa Du [1,2] and Yan Wang [1,2]

[1] School of Physics and Electronic Information, Weifang University, Weifang 261061, China; 20190026@wfu.edu.cn (F.Q.)
[2] Key Laboratory of Gallium Nitride Materials and Applications, Weifang 261061, China
[3] Shandong Leishuo Laser Technology Co., Ltd., Weifang 261201, China
[4] Beijing Institute of Technology Chongqing Innovation Center, Chongqing 401120, China
* Correspondence: xinminfan@wfu.edu.cn (X.F.); mayu@cq.bit.edu.cn (Y.M.)

Abstract

Kevlar plain-woven fabrics serve as core materials for lightweight ballistic protection, yet their microscale yarn stress evolution under in-plane shear cannot be quantitatively captured by macroscopic testing methods. This work employs static micro-Raman spectroscopy to characterize the internal stress distribution of sheared aramid textiles. A linear Raman shift–stress correlation is first established through single-yarn tensile calibration. The fabric specimen is loaded to a fixed shear angle of 30° using a picture-frame rig, after which the fixture is fully locked for undisturbed static Raman scanning. Full-field mapping results show obvious stress concentration at yarn crossover regions, with low-stress zones formed at inter-yarn gaps. The heterogeneous stress field is dominated by yarn rotation, geometric confinement and inter-yarn interfacial friction. This research provides direct mesoscale experimental data to interpret shear-induced stress redistribution and verifies the capability of micro-Raman spectroscopy for textile micromechanics characterization.

Keywords: micro-Raman spectroscopy; Kevlar plain-woven fabric; in-plane shear; yarn stress distribution

1. Introduction

Owing to their ultra-high tensile modulus, specific strength and superior impact-energy-dissipation capability, Kevlar aramid fibers are indispensable materials for ballistic-protection applications, aerospace components, and fiber-reinforced composite structures [1]. Benefiting from the interlaced warp–weft woven architecture, woven Kevlar textiles exhibit better structural stability and damage resistance compared with unidirectional laminates [2,3]. However, the global mechanical response of such fabrics is strongly coupled with microscale yarn deformation and inter-yarn interactions [4,5]. Clarifying the microscale yarn stress distribution is therefore a prerequisite for woven-architecture optimization and can further support performance analysis for ballistic-protection scenarios [6,7].

In-plane shear dominates the deformation behavior of woven fabrics under projectile impact and thermoforming loading [8]. Shear loading induces mutual yarn rotation, bending deformation, interfacial slippage, and variable yarn–yarn contact areas. These phenomena restructure internal load-transfer paths and produce localized stress concentration within woven unit cells. For plain-woven Kevlar fabrics, the originally orthogonal yarn layout undergoes continuous distortion during shear. Although macroscopic shear curves

Check for updates

Received: 15 August 2026
Revised: 29 August 2026
Accepted: 7 September 2026
Published: 10 September 2026

Copyright: © 2026 by the authors. Licensee MDPI, Basel, Switzerland. This article is an open access article distributed under the terms and conditions of the Creative Commons Attribution (CC BY) license.

can be readily acquired via picture-frame or bias-extension experiments, the underlying microscale stress evolution of individual yarns cannot be directly quantified.

Conventional shear tests only provide global structural stiffness rather than yarn-resolved stress data. Digital image correlation (DIC) can capture full-field surface strain, yet it cannot decouple the intrinsic axial stress of crimped, interlaced yarns. Numerical modeling, by contrast, relies heavily on artificial assumptions regarding yarn friction and contact behavior and often lacks direct experimental validation [9]. Consequently, direct measurement of microscale yarn stress within sheared woven fabrics remains a major technical bottleneck.

Micro-Raman spectroscopy serves as a promising non-contact micro-optical characterization tool [10]. The characteristic 1610 cm^{-1} peak of Kevlar fibers exhibits a linear blue-shift response under axial tension, enabling quantitative stress evaluation using pre-calibrated shift-stress coefficients [4,11]. Previous studies have validated Raman-based stress measurements for single Kevlar yarns under tension and out-of-plane indentation [4,11,12]. Nevertheless, few studies have adopted this technique to visualize full-field stress redistribution within fabrics subjected to in-plane shear deformation.

This work utilizes static locked-frame Micro-Raman spectroscopy to characterize yarn-scale stress distribution in plain-woven Kevlar fabrics at a fixed shear angle. Three main research objectives are outlined as follows:

(1) Calibrate the linear Raman shift-stress relationship for both warp and weft Kevlar yarns;

(2) Achieve static full-field Raman stress mapping on rigidly locked shear specimens without specimen unloading;

(3) Elucidate the micro-mechanism of stress concentration originating from contact friction at yarn crossover regions [13].

Unlike conventional characterization protocols that require specimen unloading prior to measurement, the picture-frame fixture in this study is fully tightened and locked once the target 30° shear angle is reached. Static point-by-point Raman scanning is performed directly on the deformed fabric without disturbing its configuration, so that the shear-induced stress field is well preserved for reliable mesoscale measurements.

The plain-woven Kevlar fabric studied herein consists of orthogonally interlaced warp and weft yarns, forming a periodic woven architecture with abundant yarn crossover regions. When the fabric undergoes in-plane shear deformation, the initially orthogonal yarns rotate with respect to one another, altering yarn orientation and inter-yarn contact conditions, as illustrated in Figure 1a. Such structural modifications are expected to reshape local load transfer pathways inside the woven architecture [14,15].

This non-destructive optical measurement strategy provides direct microscale experimental evidence for understanding yarn-level stress evolution within sheared woven fabrics, and may offer useful references for the design and performance optimization of ballistic-protection textile structures. Details of the experimental arrangements are described in the following section.

Conventional shear tests generally characterize the global mechanical response of woven fabrics, whereas the corresponding yarn-level stress redistribution cannot be directly observed. In the present study, the fabric was deformed to a prescribed shear angle and maintained in the fixed configuration during Raman measurement. As illustrated in Figure 1b, Raman spectra were collected at multiple locations along the yarns, and the measured Raman peak shifts were converted into local yarn stresses using the established Raman stress calibration relationship. This approach enables the spatial distribution of yarn stress to be experimentally characterized without unloading the sheared fabric.

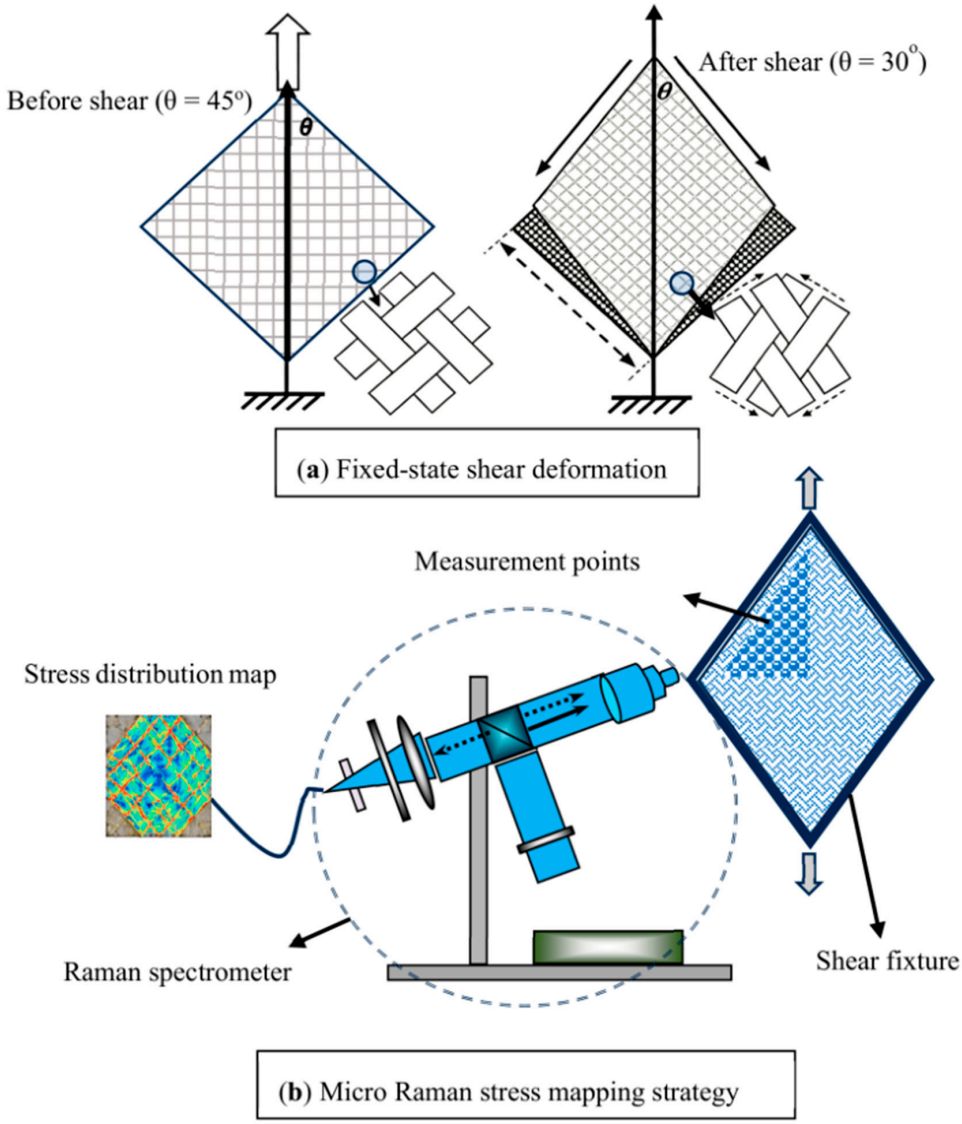


Figure 1. Schematic illustration of the experimental workflow for fixed-state shear deformation and micro-Raman stress mapping of Kevlar plain-woven fabric.

2. Materials and Methods

2.1. Materials

A plain-woven Kevlar fabric (Kevlar 49, DuPont, Wilmington, DE, USA) was selected as the research object in this study. The fabric consisted of orthogonally interlaced warp and weft yarns, forming a typical two-dimensional textile architecture. The warp and weft yarns in Kevlar 49 fabric exhibit different weaving-related dimensions, namely w_a = 1.1 mm and w_b = 1.2 mm. The woven structure provides excellent in-plane mechanical stability while allowing complex deformation through yarn rotation and interaction.

The basic structural parameters of the Kevlar fabric, including fiber type, weave pattern, yarn density, and areal density, are summarized in Table 1.

The geometric characteristics of the plain-woven Kevlar fabric were further considered in the subsequent shear and Raman measurements, as shown in Figure 2. The warp and weft yarns exhibited identical yarn densities, resulting in a nearly symmetric plain-weave architecture. The periodic unit-cell structure provided a representative region for investigating the local stress redistribution induced by shear deformation. In particular, the yarn crossover regions were considered important locations for subsequent Raman

mapping because of the geometric constraint and mechanical interaction between the warp and weft yarns.

Table 1. Material and structural parameters of the Kevlar 49 plain-woven fabric used in this study.

Parameter	Value
Fiber type	Kevlar 49 (para-aramid)
Weave pattern	Plain weave
Yarn linear density (dtex)	1420
Fiber density (g/cm^3)	1.44
Number of filaments per yarn	1000
Single-fiber diameter (μm)	12
w_a (mm)	1.2
w_b (mm)	1.1
f_a (mm)	1.0
f_b (mm)	1.0
Unit-cell size (μm × μm)	1490 × 1490

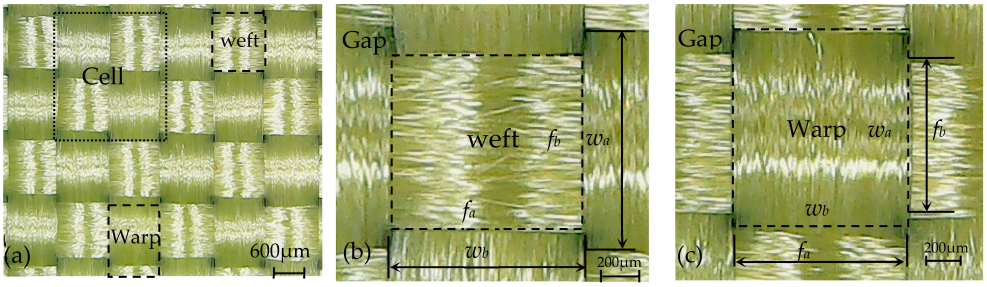


Figure 2. (**a**–**c**) Geometric dimensions of Kevlar 49 plain-woven fabric.

2.2. Raman Stress Calibration of Kevlar Yarn

Before investigating the microscale stress distribution within sheared woven fabrics, the quantitative correlation between Raman peak shift and axial stress of Kevlar yarn was calibrated. This calibration procedure was adopted from our previous published work and is briefly described below [4].

The Kevlar 49 single yarn was clamped at both ends by rope-type fixtures mounted on a micro-tensile tester (Instron 3345, Instron, Norwood, MA, USA). A portable Raman spectrometer was placed on a three-dimensional translation stage to facilitate focusing the laser spot onto the yarn surface, as shown in Figure 3.

The yarn was stretched step-by-step under load-control mode. At each load step, the Raman focusing and signal-acquisition duration were kept within 30 s to minimize viscoelastic effects of the yarn. Raman spectra were acquired using a portable Raman system (B&W Tek Prime T,B&W Tek, Newark, DE, USA), where the Raman-scattered light was collected by a back-illuminated CCD detector. The laser wavelength was 785 nm with an output power of 10 mW, and a 10× objective lens was employed. The spectral scanning range was set from 1540 cm^{-1} to 1650 cm^{-1}.

Obvious blue-shift phenomena can be observed in the Raman spectra of both warp and weft yarns under different applied loads, as illustrated in Figure 4.

The G′-band peaks of Raman spectra under different applied loads were individually fitted using Gaussian functions to extract waveform-related parameters. Subsequent normalization was performed on the extracted datasets, and the correlations between each Raman waveform parameter and applied load were obtained accordingly. Taking the warp yarn (Figure 4a) as an example, the relationships between the four Raman spectral

parameters and applied load are plotted in Figure 5a. It can be observed that the four parameters, namely x_c, W, I and A, all vary with the applied load.

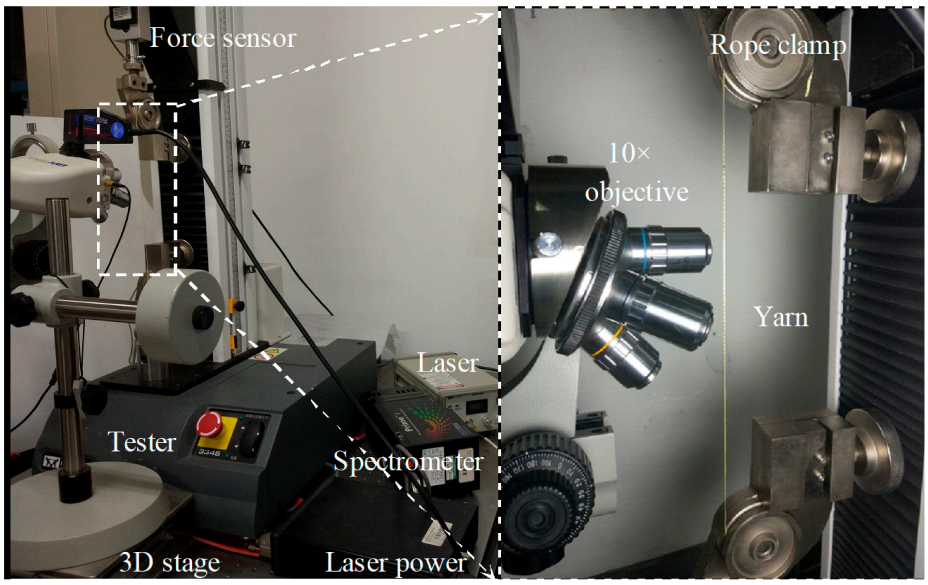


Figure 3. Device for Raman measurement of single-yarn uniaxial tensile test.

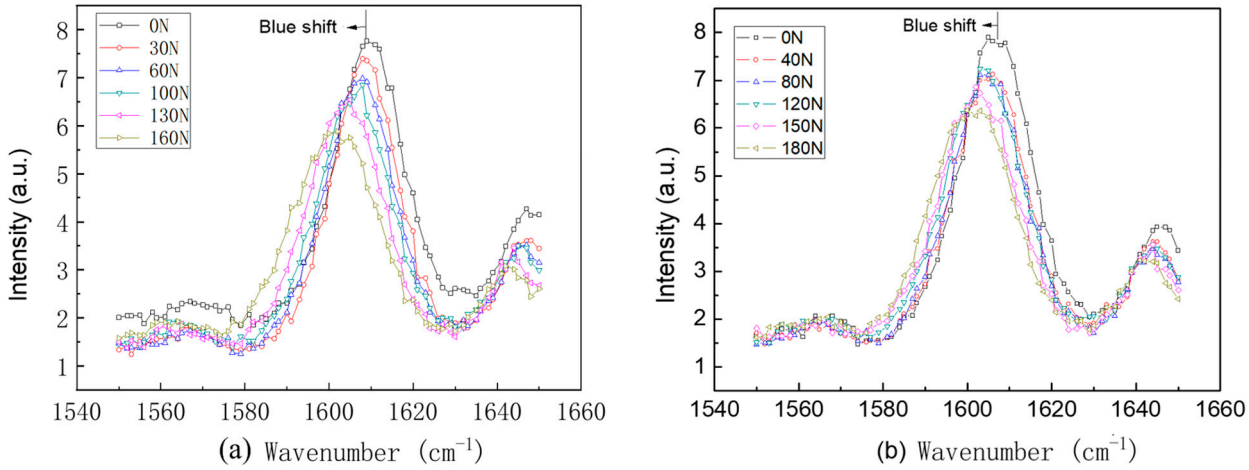


Figure 4. Raman blue shift of (**a**) warp yarn and (**b**) weft yarn under different load levels.

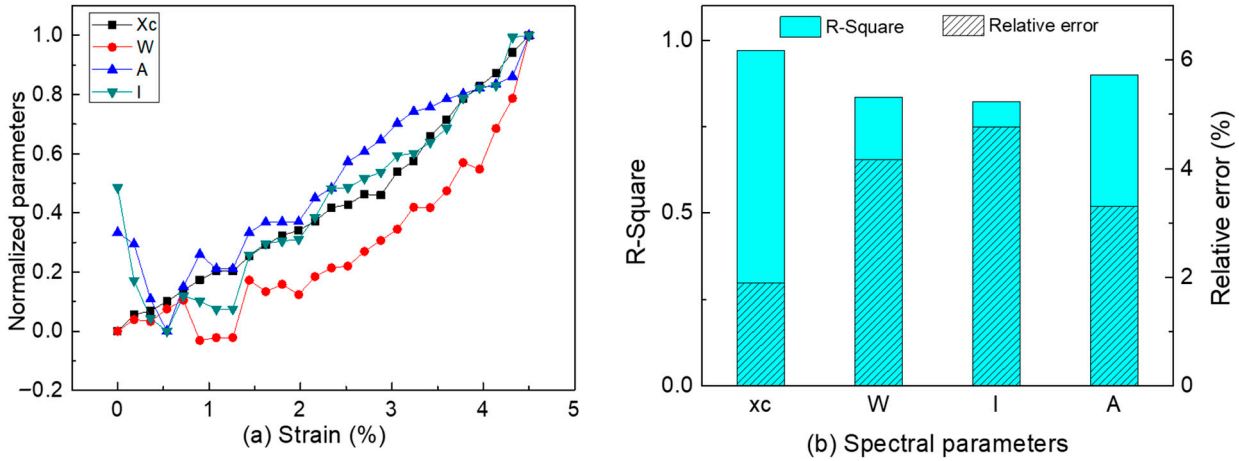


Figure 5. (**a**) Relationship between normalized Raman parameters and strain, (**b**) R-Square and relative error for each spectral parameter.

R-Square is a statistical metric evaluating the goodness-of-fit for the linear correlation between each Raman spectral parameter and applied load. The relative error, another indicator for the goodness-of-fit of linear fitting, is also presented in Figure 5b. Judging from these two indicators, the peak position x_c is the optimal spectral parameter for characterizing the load applied to the fiber. The peak area A of the Raman characteristic band ranks second in terms of linear fitting quality, while the full-width-half-maximum W shows the poorest fitting performance.

Accordingly, the peak position shift (Raman shift) of the Raman characteristic band exhibits high sensitivity and favorable linearity with respect to applied load. It is therefore necessary to further establish the proportional factor between the G'-band Raman shift and the single-yarn stress.

The Raman peak shift $\Delta\omega$ is defined as:

$$\Delta\omega = \omega - \omega_0$$

where ω_0 is the peak wavenumber under the unstressed state, and ω denotes the peak position under applied mechanical load.

A linear relationship between Raman peak shift and applied yarn stress was obtained:

$$\Delta\omega = k\sigma$$

where k is the pre-calibrated Raman shift-stress coefficient, and σ represents the axial tensile stress of the Kevlar yarn.

Batch-processing was performed on the Raman spectra in Figure 4 to extract the G′-band peak positions. By comparing these peak positions with the G′-band position obtained under zero-load condition, the Raman shift in the yarn under each corresponding load was calculated. Afterwards, the single-yarn stress was derived by dividing the tensile load by the nominal cross-sectional area of the single yarn. The relationships between Raman shift and stress for warp and weft yarns were then established separately, as shown in Figure 6.

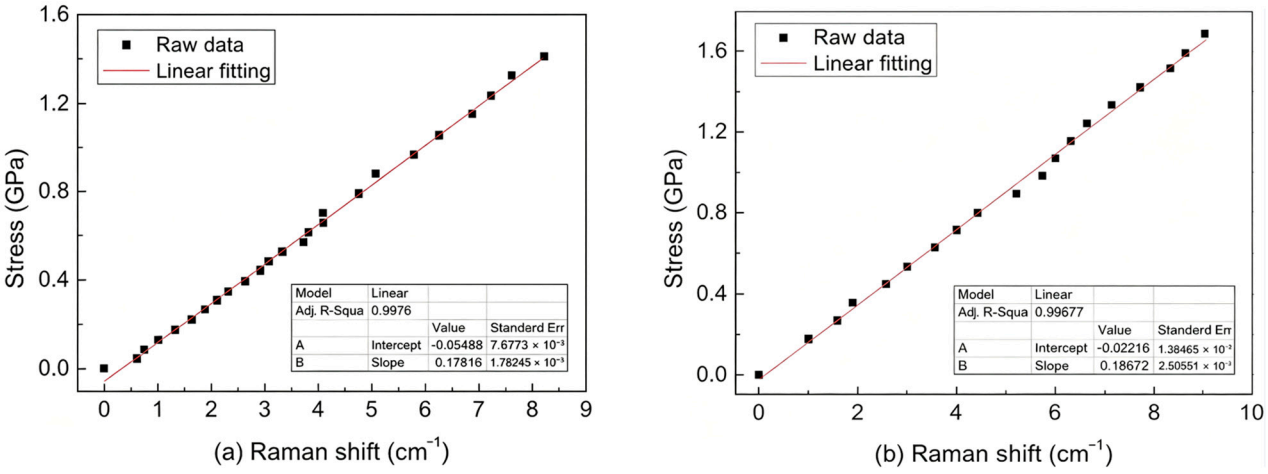


Figure 6. Relationships between Raman shift and stress of (**a**) warp yarn and (**b**) weft yarn.

Figure 6a demonstrates that the Raman shift-stress curve of the warp yarn presents an approximately linear relationship. The slope of this curve corresponds to the Raman shift-stress factor of the warp yarn, which is approximately 178.16 MPa/cm^{-1}. Similarly, the Raman shift-stress factor of the weft yarn was determined to be 186.72 MPa/cm^{-1}, as illustrated in Figure 6b.

Limited by sample preparation and long-time Raman-mapping acquisition, five single-yarn specimens were used for calibration, and one fabric specimen was subjected to a shear Raman test. Good consistency was observed among these replicates. Representative results are reported herein [11].

For the convenience of subsequent analysis, the average value of the warp- and weft-yarn Raman shift-stress factors was adopted as the unified Raman shift-stress factor for single yarns in this work, yielding a value of approximately 182.44 MPa/cm^{-1}.

It should be noted that the linear fitting of the Raman stress calibration curve yields a negative-stress intercept when the Raman shift equals zero. This intercept is a mathematical artifact induced by linear-regression deviation, and it does not correspond to real compressive stress inside the Kevlar yarn. Since this study mainly focuses on **relative stress variation** among different positions within the sheared fabric, this fitting deviation will not affect the comparative analysis of stress distribution.

2.3. Shear Deformation Experiment

The in-plane shear deformation of the Kevlar plain-woven fabric was performed using a picture-frame shear fixture. Square fabric specimens were mounted on the four edges of the fixture to ensure uniform boundary constraints during deformation. The portable Raman device (B&W Tek Prime T) was placed in front of the fabric sample. The portable Raman spectrometer is integrated with a three-axis translation stage for X-Y-Z positioning, enabling spectral acquisition at arbitrary positions on the fabric surface. The corresponding experimental setup is shown in Figure 7.

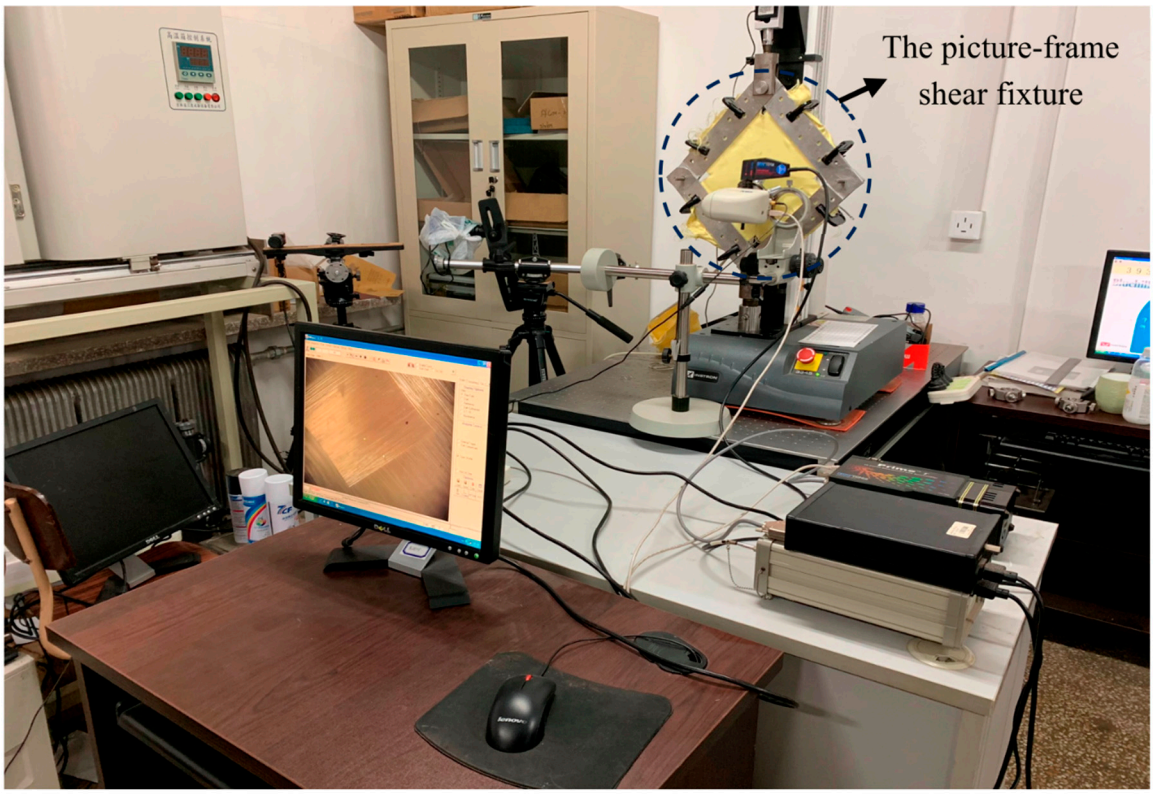


Figure 7. Experimental setup for fixed-state shear deformation and micro-Raman measurement of the Kevlar plain-woven fabric.

The picture-frame test rig illustrated in Figure 8 was employed to acquire Raman spectral data for Kevlar woven fabric. The fabric sample was rigidly secured within the picture-frame fixture. Figure 8 shows the dimensions of the Kevlar 49 fabric specimen, with

an effective area size of 180 mm × 180 mm square. However, a small square was cut at each corner of the specimen to make the original specimen a cross-shaped specimen. The purpose of this is to facilitate the free rotation of the connecting rod of the frame and prevent premature buckling of the specimen during the shearing process. During the installation of Kevlar fabric specimens onto the image frame device, it is necessary to ensure that their warp and weft fiber bundles are parallel or perpendicular to the connecting rod of the image frame device, and that the diagonal of the specimen coincides with the stretching direction. The valid deformation region of the fabric specimen was diagonally partitioned into four quadrants, with a dot matrix printed on the upper-right quadrant.

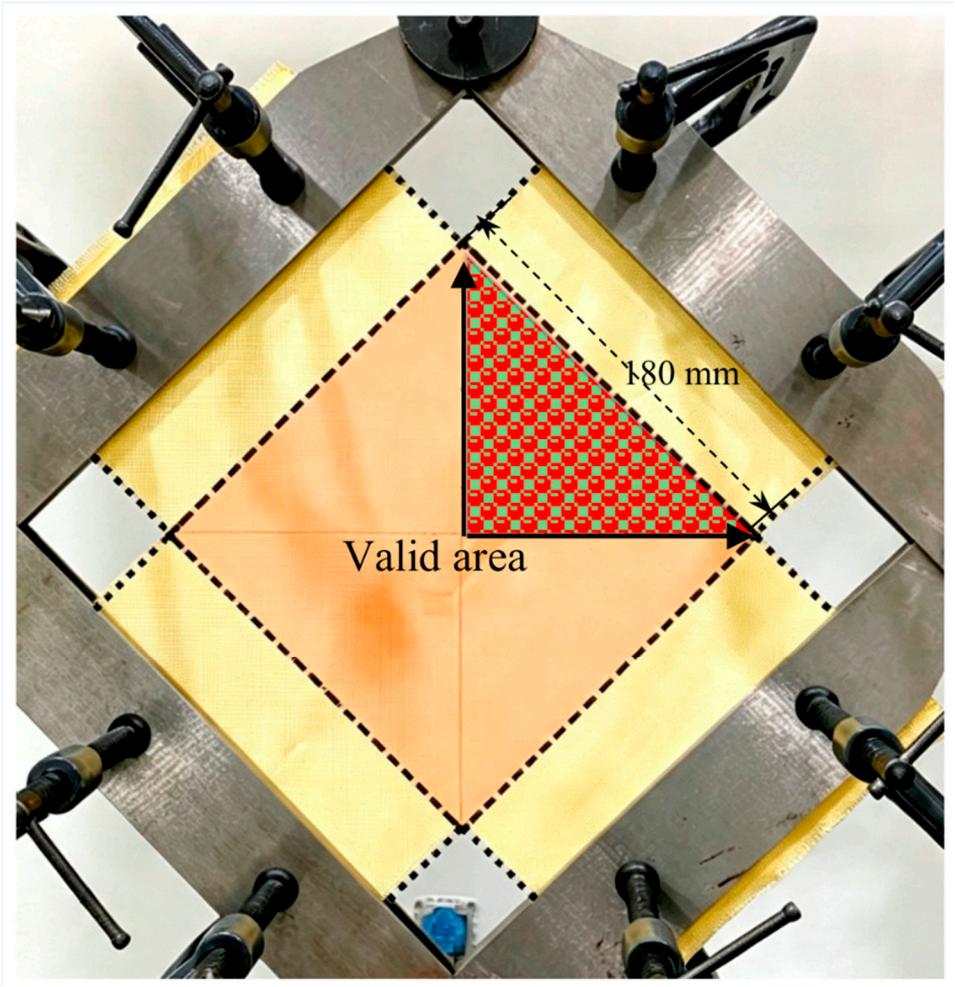


Figure 8. Picture-frame test: clamping state and Raman measurement region.

Raman measurement was performed with an excitation laser wavelength of 785 nm, a 10× objective lens, and a spectral scanning range spanning 1450 cm^{-1} to 1750 cm^{-1}. Over a laser-power range of 5 mW to 20 mW, the characteristic aramid peak of single yarn remained stable at 1610 cm^{-1}. This confirms that low-laser-power irradiation can eliminate thermal-heating artifacts during Raman testing; accordingly, a laser power of 10 mW was adopted throughout this work.

Leveraging the geometric symmetry of the picture-frame shear configuration, the Kevlar plain-woven fabric was subjected to a tensile load until a prescribed shear angle of 30° was achieved. Owing to the symmetry of both the specimen geometry and loading condition, Raman spectral acquisition was performed only within the first quadrant of the Cartesian coordinate system (xoy), corresponding to the isosceles triangular region highlighted in Figure 6b. During shear deformation, the geometry and spatial distribution

of the mapping region changed with the rotation of the warp and weft yarns, as shown in Figure 9a,b. However, the number of warp–weft crossover nodes contained within the selected region remained unchanged before and after deformation. Thus, the same set of approximately 1600 warp–weft crossover nodes could be tracked and characterized in the initial and sheared configurations, providing a consistent basis for comparing the microscale stress distribution before and after shear deformation.

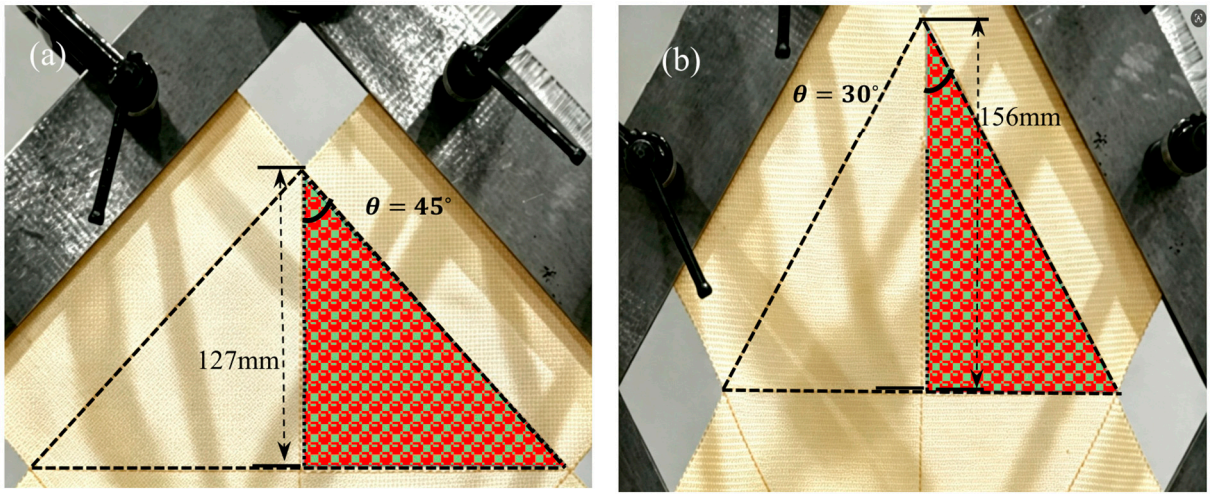


Figure 9. Fabric specimen before and after in-plane shear deformation: (**a**) initial state ($\theta = 45°$); (**b**) sheared state ($\theta = 30°$).

The prescribed shear angle of 30° was reached. The loading displacement was approximately 57 mm. At this point, the angle between the warp and weft yarns changed from 90° in the orthogonal state to 60°. At this deformation state, the shear fixture was mechanically locked to maintain the deformed configuration.

The fixed shear frame prevented macroscopic recovery and minimized stress relaxation of the yarns, allowing the deformation-induced stress distribution to be directly characterized.

After fixation, the specimen was transferred to the micro-Raman system while maintaining the original boundary conditions. Raman measurements were subsequently performed directly on the fabric surface to characterize the local stress distribution of the warp and weft yarns, with particular attention to the stress state at the warp–weft crossover regions.

A representative woven unit was selected as the Raman mapping region. The selected area contained both warp and weft yarns as well as typical yarn crossover regions. Raman spectra were collected at multiple spatial locations with a predefined scanning interval to characterize the local stress variation within the woven structure.

According to the Raman measurement scheme for fabric frame shear testing, complete Raman spectroscopy measurements inside the shear frame at different shear angles measuring up to 30 degrees. Benefiting from the relatively uniform deformation feature within the valid shear region of the picture-frame specimen, Raman spectral acquisition was performed over a dot-matrix area covering fabric unit cells. The focus diameter of the laser with the 10× magnification objective lens is approximately 85 μm, which is much smaller than the dimension of yarn-to-yarn intersections. As illustrated in Figure 10, a 3 × 3 dot-matrix with nine independent Raman measurements was performed within each warp–weft yarn crossover point. The nine acquired Raman datasets were averaged to obtain the representative mean Raman shift for that yarn intersection. During full-field mapping, manual focal adjustment was conducted for every measurement spot. The sampling points were arranged continuously without spatial gaps or skipped woven unit cells.

This measurement strategy enables a smooth transition of the stress field across adjacent unit cells and avoids artificial discontinuities in stress distribution. All Raman spectral data were stored with their corresponding position indices. As shown in Figure 10b, the raw Raman spectra collected from nine sampling spots within a typical yarn intersection under 30° shear deformation are presented. The averaging operation is subsequently performed on the Raman-shift data obtained from all other nodes.

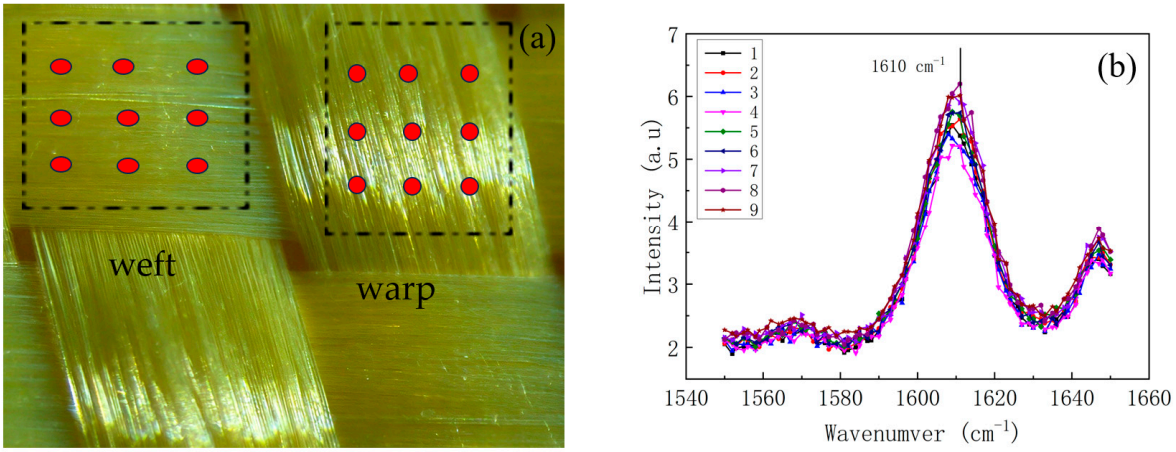


Figure 10. (**a**) Raman spectra of 3 × 3 lattices on warp surface and weft surface. (**b**) The corresponding Raman spectrum of a typical intersection point under 30-degree shear deformation.

3. Results and Discussion

3.1. Stress Redistribution After Shear Deformation

By comparing the Raman characteristic peaks of Kevlar 49 aramid fibers at 1610 cm^{-1} under no load, the corresponding Raman frequency shift under load can be obtained and then converted into the corresponding full-field stress distribution through the Raman frequency shift-stress factor of the yarn, as shown in Figure 11.

Unlike indirect strain measurement techniques such as DIC, the micro-Raman spectroscopy coefficient enables direct conversion of collected Raman spectral signals into real axial stress of individual interlaced yarns. The calibration eliminates ambiguity caused by fabric crimp and complex mesostructures, verifying that micro-Raman spectroscopy can reliably quantify the internal yarn stress distribution inside sheared Kevlar woven architectures.

After the fabric is deformed and rigidly locked at a shear angle of 30°, the overall stress field undergoes significant redistribution and presents a typical diagonal concentration characteristic. Severe local stress concentration occurs exclusively at the two opposite corners—the fixed corner and the loaded corner—which serve as the direct loading and constraint boundaries of the picture-frame fixture. From the two clamped corners toward the interior of the specimen, the yarn axial stress decreases rapidly along the loading diagonal. In the vast central region of the fabric, the stress level remains relatively uniform and low, as yarns in this area mainly undergo in-plane rotation rather than axial tension. The other two free corners, which are free of external constraints, maintain the lowest stress state in the whole specimen.

The Raman stress proportional factor is calibrated using isolated Kevlar 49 single yarns. For yarns embedded within the sheared plain-woven fabric, this calibration factor is adopted on the following basis. The isolated yarn and in-fabric yarn share identical fiber material, molecular composition and fiber assembly. The G′-band Raman shift in Kevlar 49 primarily reflects axial tensile stress of molecular chains, which is an intrinsic material response. Under picture-frame shear deformation, yarns inside the fabric are

predominantly subjected to axial tension, although local transverse compressive contact exists at yarn–yarn crossover locations. It should be noted that local transverse contact stress at interlacing points cannot be resolved in our current Raman measurement, which may bring minor deviations for local stress evaluation and represents a limitation of the present test method.

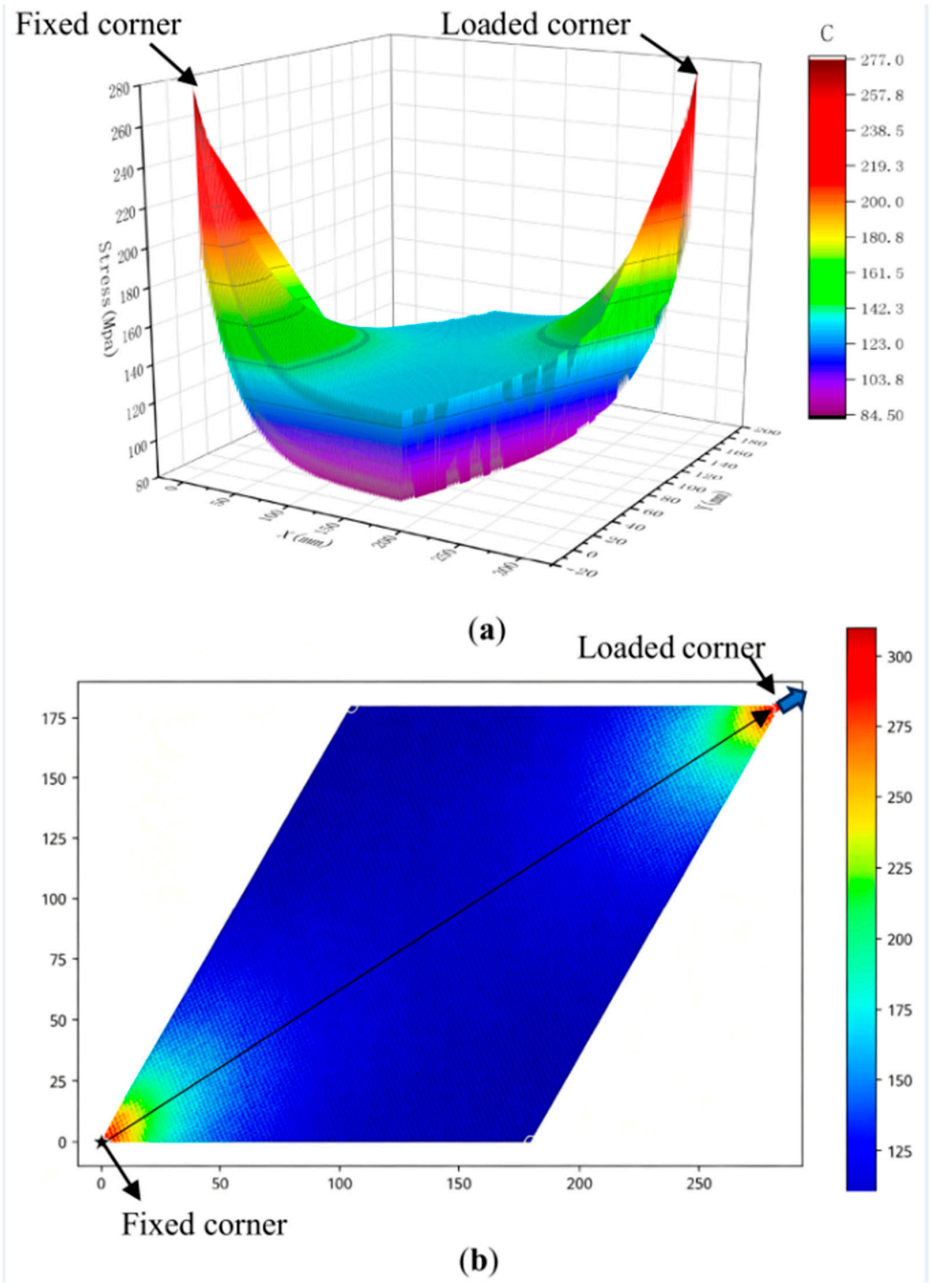


Figure 11. Full-field yarn stress distribution contours of Kevlar plain-woven fabric fixed 30° shear deformation state after fixture locking: (**a**) 3D surface of von-Mises equivalent stress; (**b**) 2D contour of von-Mises equivalent stress.

This spatial distribution pattern demonstrates that the in-plane shear load of the picture-frame test is mainly borne by the yarns near the loading diagonal, and the boundary clamping effect dominates the macroscale stress concentration. The shear deformation in the central fabric domain is accommodated mostly by yarn rotation, so the axial tensile stress generated therein is limited. This kind of heterogeneous stress distribution with localized

corner concentration cannot be captured by global mechanical curve tests or surface strain-only DIC measurements, verifying the advantage of full-field stress characterization.

It should be noted that the stress concentration appearing at fabric corners originates from combined effects. On one hand, the intrinsic mesoscale mechanical behavior of plain-woven fabric, including yarn slippage, inter-yarn friction and contact compaction under large shear deformation, contributes to local stress build-up. On the other hand, the clamping boundary conditions of the picture-frame setup will introduce additional local stress at specimen edges. In our present test, the stress magnitude at the corner region is jointly governed by both factors, and it is difficult to completely decouple their individual contributions under quasi-static locked-shear conditions.

It should be noted that full-field Raman mapping for woven fabric under shear loading requires extremely long acquisition time. For this reason, only reliable measurement results at 30° shear angle are reported in the current study, and multi-angle tests will be pursued in future work.

3.2. Effect of Yarn Crossover on Stress Concentration

To quantitatively describe the stress variation along the load transmission path, Figure 12 plots the von-Mises equivalent stress distribution along the loading diagonal from the fixed corner to the loaded corner. The curve exhibits a typical symmetric U-shaped feature: the stress reaches its peak at both ends of the diagonal, with a maximum value of approximately 277 MPa at the fixed and loaded corners; as the distance from the corner increases, the stress decreases rapidly in a nearly exponential decay manner; in the middle section, accounting for about 70% of the diagonal length, the stress maintains a stable low level of around 135–150 MPa with small fluctuations.

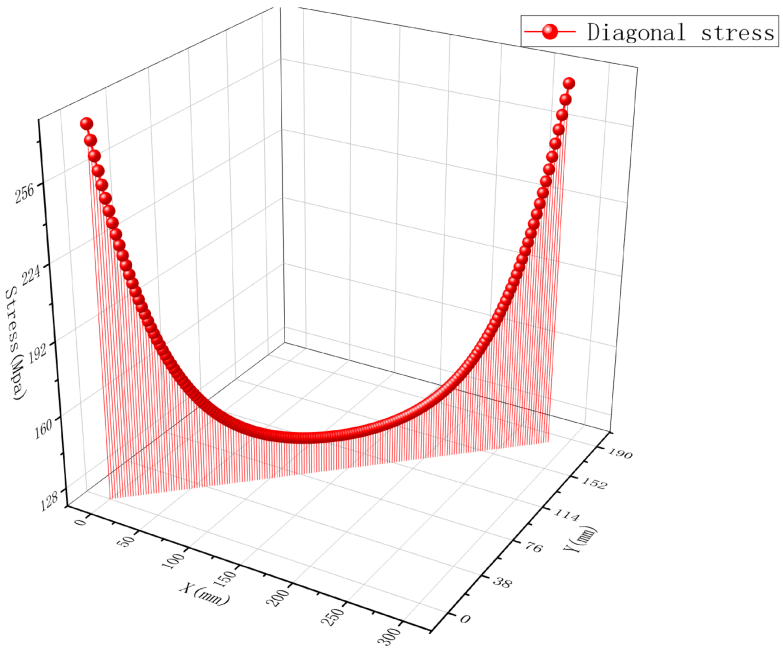


Figure 12. Three-dimensional profile of von-Mises equivalent stress along the loading diagonal from fixed corner to loaded corner under 30° locked shear deformation.

This U-shaped distribution directly reflects the attenuation law of the boundary constraint effect. The strong clamping and tension at the corner induce significant axial stretching of yarns, forming a local high-stress zone. With stress transferred inward along the yarn, part of the deformation is gradually released through yarn rotation, resulting in continuous stress attenuation. After entering the central region where yarn rotation

is sufficient, the stress tends to be stable, and the fabric mainly bears shear load in the form of yarn rotation without further obvious stress accumulation. From the macro full-field perspective, stress is concentrated at the loading boundaries; from the meso unit-cell perspective, the internal stress of a single yarn also shows obvious heterogeneity due to the interlaced structure. Under the initial undeformed condition, warp and weft yarns intersect at a standard 90° orthogonal angle without mutual extrusion. When subjected to 30° in-plane shear, relative rotation occurs between interlaced yarns, and the intersection angle decreases from 90° to 90–γ (γ = 30°). The yarn rotation compresses the contact area at each crossover point, drastically enhancing interfacial extrusion and frictional interaction between warp and weft yarns.

The micro-Raman stress mapping of the unit cell directly reflects the consequence of enhanced inter-yarn contact: maximum axial stress concentrates exactly at the yarn crossover region. Stress values gradually decay along the yarn axis away from the intersection point, showing medium stress at the near-crossover transition zone, and the lowest tensile stress on the free yarn segments without contact constraint. This spatially differentiated stress distribution confirms that geometric rotation of interlaced yarns under shear is the root cause of localized stress concentration inside woven fabrics at the mesoscale. The rigid contact constraint at crossover points restricts relative sliding and transfers shear load into axial tension of the yarn body.

To quantitatively evaluate the influence of interlaced crossover geometry on mesoscale stress accumulation, the average yarn stresses extracted from three typical structural positions (crossover region, near-crossover zone, and free yarn segment) under the fixed 30° shear state are compared statistically. Specifically, the crossover region possesses the highest average axial stress, reaching approximately 152 MPa. The near-crossover zone exhibits a moderate average stress of around 91 MPa, about 40% lower than that at the crossover position. The free yarn segment maintains the minimum stress level of merely 38 MPa, only one-quarter of the stress measured at yarn intersections.

The obvious stress gap between contact and non-contact regions fully demonstrates that yarn crossover acts as the core load-transfer node within the woven architecture. The geometric interlocking effect generated by yarn rotation under shear creates compressive contact stress at intersections, which is balanced by axial tensile stress along the yarn length. Without the constraint from adjacent crossing yarns, free segments cannot bear transferred shear load, resulting in far lower tensile stress.

Combined with the macro full-field results, it can be found that the stress concentration in sheared Kevlar fabrics presents a dual-scale feature: at the specimen scale, stress is concentrated at the loading diagonal corners driven by boundary constraints; at the yarn unit-cell scale, stress is further concentrated at the crossover points driven by inter-yarn contact constraints. The crossover contact constraint dominates the inter-yarn load transfer process and controls the magnitude of local stress concentration at the mesoscale.

3.3. Mechanism of Yarn Stress Redistribution

Combining the full-field Raman mapping results, diagonal stress distribution analysis and microscale unit-cell investigation, a multiscale stress redistribution mechanism under in-plane shear is proposed. The evolution process from global deformation to localized stress concentration can be divided into three stages, as illustrated in Figure 13.

Stage 1: Initial orthogonal woven structure.

In the absence of external shear load, warp and weft yarns intersect at a perfect 90° angle. There is only weak residual contact pressure at crossover points, and almost no extra axial tension exists inside either yarn set. The internal stress field of the fabric remains homogeneous and close to zero at both the macro- and mesoscales.

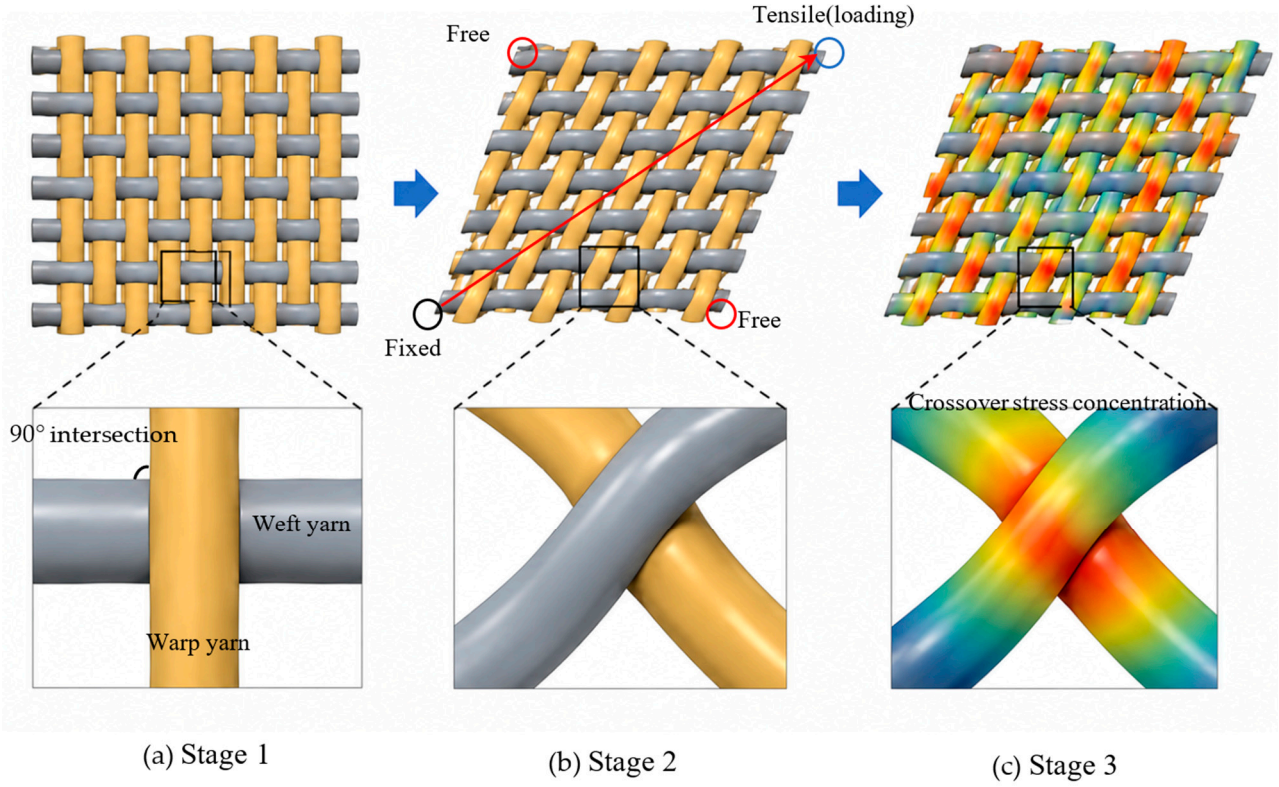


Figure 13. Schematic illustration of the three-stage multiscale yarn stress redistribution mechanism for plain-woven Kevlar fabric subjected to in-plane shear deformation. (**a**) Stage 1: Initial orthogonal woven structure without external shear load; (**b**) Stage 2: Global shear deformation and mutual rotation of warp–weft yarns; (**c**) Stage 3: Dual-scale stress concentration under sustained mechanical constraints.

Stage 2: Global shear deformation and yarn mutual rotation.

When the picture-frame fixture is loaded to a 30° shear angle, the global frame deformation drives the specimen into a diamond shape and induces relative rotation between orthogonal warp and weft yarns. At the macroscale, the tensile load is first transmitted to the two diagonal corners of the specimen, forming initial boundary stress concentration. At the mesoscale, the intersection angle between yarns reduces, and the contact area at each crossover expands, producing enhanced interfacial extrusion and friction between crossing yarns. External shear displacement is converted into internal contact force within the woven mesostructure.

Stage 3: Dual-scale stress concentration under sustained constraints.

After the fixture is fully locked to retain the shear geometry, stable constraints are maintained at both the specimen boundary and the yarn crossover points. At the macroscale, continuous clamping at diagonal corners keeps the yarns in a high-tension state near the loading path, and stress attenuates gradually toward the central region with the release of rotational deformation. At the mesoscale, contact friction at crossover points restricts relative sliding between yarns, forcing shear load to transmit along the yarn axial direction. Significant tensile stress accumulates at the crossover nodes, while stress gradually attenuates toward free yarn segments far from interlaced contact.

This three-stage evolution mechanism clarifies the intrinsic coupling relationship among macro boundary constraint, yarn geometric rotation, inter-yarn interfacial contact and heterogeneous stress field formation, providing direct multiscale experimental support for explaining the energy absorption and damage initiation behavior of ballistic woven fabrics under shear-dominated impact loads.

4. Conclusions

In this work, static locked-frame micro-Raman spectroscopy was adopted to quantitatively characterize the microscale yarn stress distribution of Kevlar plain-woven fabric under a fixed 30° in-plane shear deformation. Key conclusions are summarized as follows:

Micro-Raman spectroscopy combined with a pre-calibrated linear Raman shift-stress coefficient successfully realizes direct, non-contact measurement of axial stress for individual interlaced yarns inside woven Kevlar fabrics. The stable linear correlation between peak blue shift and yarn tensile stress eliminates the indirect conversion error of macroscopic strain testing methods and enables full-field visualization of mesoscale stress heterogeneity in textile architectures.

The static testing scheme with a fully locked shear fixture effectively avoids specimen unloading and subsequent stress relaxation during optical measurement. The shear-induced stress field can be completely preserved without structural disturbance, which overcomes the major limitation of traditional characterization workflows that require releasing deformation before sampling. This simplified static measurement strategy greatly reduces experimental workload while acquiring reliable steady-state stress data.

The full-field stress of the sheared fabric presents a typical diagonal concentration distribution at the specimen scale, with the highest stress at the fixed and loaded corners and a uniform low-stress level in the central region. Along the loading diagonal, the stress shows a symmetric U-shaped distribution with peak values at both ends and a stable plateau in the middle. At the meso unit-cell scale, severe local stress concentration primarily concentrates at yarn crossover regions, while stress values decrease sequentially from crossover zones to near-crossover transition areas and free yarn segments.

Relative yarn rotation under shear is the fundamental origin of uneven stress accumulation, which induces dual-scale stress concentration: at the macroscale, boundary clamping drives diagonal stress concentration; at the mesoscale, enhanced interfacial contact friction at crossover points further amplifies local stress. Geometric interlocking at crossover nodes dominates the inter-yarn load transfer pathway inside the woven structure.

A three-stage multiscale yarn stress redistribution mechanism (initial orthogonal structure → global shear deformation and yarn mutual rotation → dual-scale stress concentration under sustained constraints) is established based on full-field Raman mapping results. This research supplies direct microscale experimental evidence to interpret the micromechanical deformation mechanism of aramid woven fabrics under shear loading, and the proposed static micro-Raman characterization method can be extended to further studies on ballistic impact energy dissipation and textile structural optimization.

Author Contributions: Conceptualization, F.Q., X.F., Y.W. and Y.M.; validation, J.Z., Z.D. and Y.W.; investigation, F.Q., X.F. and Y.M.; resources, F.Q., X.F., J.Z. and Z.D.; writing—original draft preparation, F.Q., X.F. and Y.W.; writing—review and editing, F.Q., X.F. and J.Z.; visualization J.Z. and X.F.; supervision, F.Q., X.F. and Z.D.; funding acquisition, F.Q. and X.F. All authors have read and agreed to the published version of the manuscript.

Funding: This work was funded by Shandong Advanced Optoelectronic Chip Innovation and Entrepreneurship Community project (No. 20210701) and the 2024 Weifang Science and Technology Development Plan Project (2024GX018). This research was funded by the Shandong Province Key Research and Development Program (Science and Technology Smes Innovation Ability Improvement Project) (grant no. 2024TSGC0553) and the Weifang Science and Technology Development Program (Competitive Innovation Platform) (grant no. 2024JZ0021).

Data Availability Statement: The raw data supporting the conclusions of this article will be made available by the authors on request.

Conflicts of Interest: Yu Ma was affiliated with Beijing Institute of Technology Chongqing Innovation Center. The remaining authors declare that the research was conducted in the absence of any commercial or financial relationships that could be construed as a potential conflict of interest.

References

1. Parthenios, J.; Katerelos, D.G.; Psarras, G.C.; Galiotis, C. Aramid fibers: A multifunctional sensor for monitoring stress/strain fields and damage development in composite materials. *Eng. Fract. Mech.* **2002**, *69*, 1067–1087. [CrossRef]
2. Karahan, M.; Ku, A.; Eren, R. An investigation into ballistic performance and energy absorption capabilities of woven aramid fabrics. *Int. J. Impact Eng.* **2008**, *35*, 499–510. [CrossRef]
3. Wu, H.; Zhao, Z.; Bai, Y.; Fang, S.; Ma, D.; Zhang, C. Intralaminar hybrid configurations on the impact resistance of Carbon/Kevlar plain-woven composite plates. *Thin-Walled Struct.* **2025**, *209*, 107986. [CrossRef]
4. Qin, F.; Lei, Z.; Ma, Y.; Fang, Q.; Bai, R.; Qiu, W.; Yan, C.; Feng, Y. Stress transfer of single yarn drawing in soft fabric studied by micro-Raman spectroscopy. *Compos. Part A-Appl. Sci. Manuf.* **2018**, *112*, 134–141. [CrossRef]
5. Sharma, P.; Mali, H.S.; Dixit, A. Mode-II interlaminar fracture toughness characterization of woven carbon–Kevlar interyarn hybrid textile composites. *Iran. Polym. J.* **2025**, *34*, 1981–2001. [CrossRef]
6. Cunniff, P.M. An analysis of the system effects in woven fabrics under ballistic impact. *Text. Res. J.* **1992**, *62*, 561–575. [CrossRef]
7. Farajyar, S.; Wan, H.; Wang, Y. Finite element analysis of ballistic impact on Kevlar-29/epoxy composites with varying layer configurations. *Int. J. Impact Eng.* **2026**, *208*, 104789. [CrossRef]
8. Luo, X.; Tan, H.; Wu, G.; Wang, S. Experimental investigation of in-plane shear performance for F-12 aramid fabric. *Acta Mater. Compos. Sin.* **2018**, *35*, 591–598.
9. Viita, D. Static and Dynamic Raman Spectroscopic Studies of Woven Body Armour. Master's Thesis, University of Manchester, Manchester, UK, 2014.
10. Lei, Z.K. Stress transfer of a Kevlar 49 fiber pullout test studied by micro-Raman spectroscopy. *Appl. Spectrosc.* **2013**, *67*, 895–902. [CrossRef] [PubMed]
11. Lei, Z.K.; Qin, F.Y.; Fang, Q.C.; Bai, R.X.; Qiu, W.; Chen, X. Full-field fabric stress mapping by micro-Raman spectroscopy in a yarn push-out test. *Appl. Opt.* **2018**, *57*, 924–930. [CrossRef] [PubMed]
12. Kukle, S.; Lazov, L.; Lohmus, R.; Briedis, U.; Adijans, I.; Bake, I.; Dunchev, V.; Teirumnieka, E. The impact of CO_2 laser treatment on Kevlar KM2+ fibres: Fabric surface morphology and yarn pull-out resistance. *Polymers* **2025**, *17*, 2931. [CrossRef] [PubMed]
13. Mirmohammadi, S.M.; Najar, S.S.; Dolatabadi, M.K. Energy absorption of ballistic impact in hybrid Kevlar/Polypropylene woven fabric composites preloaded under simple shear mode: Response surface methodology modeling utilizing a Box-Behnken design. *Polym. Compos.* **2025**, *46*, 3745–3758. [CrossRef]
14. Ergün, S.; Özsoy, M.S.; Bora, M.Z. Tribological performance of Glass/Kevlar hybrid epoxy composites: Effects of pressurized water-immersion aging under reciprocating sliding wear. *Polymers* **2025**, *17*, 2944. [CrossRef] [PubMed]
15. Gandham, R.V.; Krishnan, S.; Lore, S. Analysis of vibration behavior of 3D woven hybrid carbon-Kevlar composite laminates. In *AIP Conference Proceedings*; AIP Publishing: Melville, NY, USA, 2025; Volume 3259, p. 80001.

Disclaimer/Publisher's Note: The statements, opinions and data contained in all publications are solely those of the individual author(s) and contributor(s) and not of MDPI and/or the editor(s). MDPI and/or the editor(s) disclaim responsibility for any injury to people or property resulting from any ideas, methods, instructions or products referred to in the content.